THE JOURNAL OF PHYSICAL CHEMISTRY B

Article

pubs.acs.org/JPCB

Hydrogen Bond Asymmetric Local Potentials in Compressed Ice

Yongli Huang,[†] Zengsheng Ma,[†] Xi Zhang,[‡,§] Guanghui Zhou,[¶] Yichun Zhou,[†] and Chang Q. Sun*[,†,‡,§]

[†]Key Laboratory of Low-dimensional Materials and Application Technology (Ministry of Education) and Faculty of Materials, Optoelectronics and Physics, Xiangtan University, Xiangtan 411105, China

[‡]NOVITAS, School of Electrical and Electronic Engineering, Nanyang Technological University, Singapore 639798

[§]Center for Coordination Bond and Electronic Engineering, College of Materials Science and Engineering, China Jiliang University, Hangzhou 310018, China

[¶]Department of Physics and Key Laboratory for Low-Dimensional Structures and Quantum Manipulation (Ministry of Education), Hunan Normal University, Changsha 410081, China

Supporting Information

ABSTRACT: A combination of the Lagrangian mechanics of oscillators vibration, molecular dynamics decomposition of volume evolution, and Raman spectroscopy of phonon relaxation has enabled us to resolve the asymmetric, local, and short-range potentials pertaining to the hydrogen bond (O:H−O) in compressed ice. Results show that both oxygen atoms in the O:H−O bond shift initially outwardly with respect to the coordination origin (H), lengthening the O−O distance by 0.0136 nm from 0.2597 to 0.2733 nm by Coulomb repulsion between electron pairs on adjacent oxygen atoms. Both oxygen atoms then move toward right along the O:H−O bond by different amounts upon being compressed, approaching identical length of 0.11 nm. The van der Waals potential $V_L(r)$ for the O:H noncovalent bond reaches a valley at −0.25 eV, and the lowest exchange $V_H(r)$ for the H−O polar-covalent bond is valued at −3.97 eV.

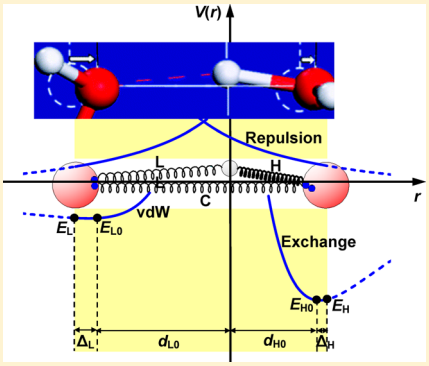

1. INTRODUCTION

Water and ice have attracted much attention because of their anomalous behavior being related to issues from galaxy to geology, climate, biology, and our daily lives.[1−8] As the basic structural unit, the hydrogen bond (O:H−O or H-bond)[9] relaxes in length and stiffness unexpectedly under applied stimulus such as heating,[10,11] salting,[12] clustering,[1,13,14] charging,[15] and compressing.[16−18] Contributions have been made computationally,[19−23] experimentally,[24−26] and theoretically[27,28] to the understanding of water and ice based on the polarizable or the nonpolarizable models,[29,30] including the TIP*n*P (*n* varies from 1 to 5) series[29−33] and density functional theory (DFT) with[34] and without[35] dispersion corrections or inclusion of hydrogen bonding and van der Waals (vdW) interactions. Using DFT and molecular dynamics (MD) calculations, we have been able to reproduce multiple anomalies demonstrated by compressed ice,[18] by water ice at cooling,[11] and by water molecules with fewer than four neighbors[14] that can be found at the edges of the hydrogen-bonded networks[14] with limited information about the details of the inter- and intramolecular interactions.

Length symmetrization of the O:H−O bond in ice happens under 59−60 GPa compression with mechanism that remains unclear.[17,36,37] In 1972, Holzapfel[38] predicted that, under pressure, hydrogen bonds might be transformed from the highly asymmetric O:H−O configuration to a symmetric state in which the H proton lies midway between the two O ions, leading to a nonmolecular symmetric phase of ice X. This prediction was numerically confirmed in 1998 by Benoit and co-workers[17] who proposed that the "translational proton quantum tunneling under compression" dominates this phenomenon. In the same year, Goncharov et al.[39] confirmed experimentally that proton symmetrization happens under 60 GPa at 100 K, as no further phonon relaxation could be resolved even though the pressure is increased. Teixeira[37] suggested that as the oxygen atoms are forced together, the potential energy changes from a symmetric double to a single well, making the "fluctuated H proton"[9] to be certain in position. Wernet et al.[40] proposed an asymmetric H-bonding model which Soper[41] investigated by assuming different charges on the hydrogen ions in order to create an asymmetry and investigate whether that could be supported by diffraction data. Similar attempts have been carried out by Wikfeldt et al.[42] and Leetmaa et al.[43] However, this asymmetric potential assumption could not be certain at that point of time as X-ray/neutron diffraction and IR/Raman are insensitive to the interatomic potentials. Nilsson and Pettersson[44] and Kuhne and Khaliullin[45] also addressed the presence of the asymmetric potentials in liquid water.

The objective of this work is to explore the potential paths for the proton symmetrization of the segmented O:H−O bond of ice under compression. This was done by a combination of

Received: August 5, 2013
Revised: October 1, 2013
Published: October 3, 2013

Lagrangian mechanics of lattice vibration,[46−48] MD decomposition of the volume evolution, and Raman measurements of phonon relaxation dynamics of ice under compression. With the MD and Raman derived data of the segmental length d_x and vibration frequency ω_x (x = L and H represent the O:H vdW noncovalent and the H−O polar-covalent bond, respectively) of the O:H−O bond[3−6] as input, we are able to determine the force constants, the potential well depths, and the bond energy of each part of the O:H−O bond as well as their pressure dependence. We have therefore resolved the local asymmetric potentials of H-bond pertaining to compressed ice.

2. PRINCIPLES

2.1. Asymmetric Short-Range Interactions. A quasi-linear H-bond is used for simplicity because the O:H−O bond angle in ice is valued at 170° and above.[11] By averaging the surrounding background long-range interactions of H_2O molecules, protons, and the nuclear quantum effect on fluctuations,[49,50] we focus on the short-range interactions in a O:H−O bond with H atom being taken as the coordination origin.[14] The short-range interactions include the vdW force limited to the O:H bond,[51] the exchange interaction in the H−O polar-covalent bond,[52] and the Coulomb repulsion between the lone and the shared electron pairs attached to the adjacent oxygen ions:

$$V_L(r_L) = V_{L0}\left[\left(\frac{d_{L0}}{r_L}\right)^{12} - 2\left(\frac{d_{L0}}{r_L}\right)^{6}\right] \quad \text{(L-J potential } (V_{L0}, d_{L0})\text{)}$$

$$V_H(r_H) = V_{H0}[e^{-2\alpha(r_H - d_{H0})} - 2e^{-\alpha(r_H - d_{H0})}] \quad \text{(Morse potential } (\alpha, V_{H0}, d_{H0})\text{)}$$

$$V_C(r_C) = \frac{q_{\cdot}q_{-}}{4\pi\varepsilon_r\varepsilon_0 r_C} \quad \text{(Coulomb potential } (q_{\cdot}, q_{-})\text{)} \tag{1}$$

where V_{L0} and V_{H0}, commonly denoted E_{L0} and E_{H0}, are the potential well depths, or bond energies, of the respective bond. r_x and d_{x0} (x = L, H, and C) denote the interionic distances (corresponding the length of the springs) at arbitrary position and at equilibrium, respectively. The α parameter determines the width of the potential well. ε_r = 3.2 is the relative dielectric constant of ice. $\varepsilon_0 = 8.85 \times 10^{-12}$ F/m is the vacuum dielectric constant. The $q_{\cdot}$ and q_{-} denote the lone and the shared electron pairs on oxygen ions. We chose potentials for the interaction by considering least number of adjustable parameters. It is unnecessary to tell which potential is better than the other as we are concentered about the equilibrium coordinates of bond length and bond energy. Because of the short-range nature of the interactions, only the solid lines in the shaded area for the basic O:H−O unit in Figure 1 are effective. One must switch off a particular potential and on the other immediately when one moves to the boundary of the region. No spatial decay of any potential is allowed in the irrespective regime.

The d_{x0} is the interatomic distance at equilibrium without the involvement of Coulomb repulsion. The involvement of the Coulomb repulsion dislocates both O ions slightly outwardly by Δ_x from their respective ideal equilibrium positions, shifting the atomic distance from d_{x0} to $d_x = d_{x0} + \Delta_x$. The Coulomb repulsion raises the potential well depths of the O:H and the H−O from E_{x0} to E_x by the same amount.

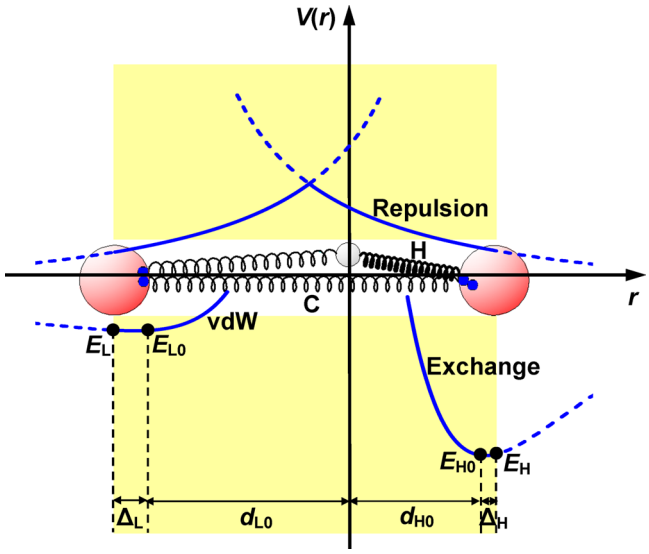

Figure 1. Schematic illustration of the segmented O:H−O bond with springs representing the short-range interactions with H atom being the coordination origin. The intramolecular exchange interaction is limited to the H−O bond (H; right-hand side). The intermolecular vdW force is limited to the O:H bond (L; left-hand side). The interelectron-pair Coulomb repulsion (repulsion) force is limited to region between adjacent O−O (C). The larger red spheres denote oxygen ions and the smaller gray sphere denotes hydrogen proton. The pair of dots on oxygen in the left denote the electron lone pair the pair of dots on the right denotes the bonding pair. The Coulomb repulsion pushes both O ions away from their ideal equilibrium positions and up a little in energy. Compression shortens and stiffens the O:H bond and meanwhile lengthens and weakens the H−O bond through repulsion toward length symmetrization.[18]

2.2. Lagrangian Oscillating Dynamics. The segmented O:H−O bond is taken as two asymmetric oscillators coupled by the Coulomb interaction and bridged by the H atom at the coordination origin. The reduced mass of the H_2O:H_2O oscillator is $m_L = 18 \times 18/(18 + 18)m_0 = 9m_0$ and that of the H−O oscillator is $m_H = 1 \times 16/(1 + 16)m_0 = 16/17m_0$ with m_0 being the unit proton mass of 1.66×10^{-27} kg. The motion of the coupled, asymmetric O:H−O oscillators follows the Lagrangian equation:[46]

$$\frac{d}{dt}\left(\frac{\partial L}{\partial(dq_x/dt)}\right) - \frac{\partial L}{\partial q_x} = Q_x \tag{2}$$

The Lagrangian $L = T - V$ consists of the total kinetic energy T and the total potential energy V. Q_x denotes the generalized nonconservative forces. Here, it is the compression force f_P. The time-dependent $q_x(t) = u_L$ and u_H represents the generalized variables, denoting the displacements of O atoms from their equilibrium positions in the springs L and H. The kinetic energy T consists of two terms, as the H is the coordination origin

$$T = \frac{1}{2}\left[m_L\left(\frac{du_L}{dt}\right)^2 + m_H\left(\frac{du_H}{dt}\right)^2\right] \tag{3}$$

The potential energy V is composed of three terms: the vdW interaction $V_L(r_L) = V_L(d_{L0} - u_L)$, the exchange interaction $V_H(r_H) = V_H(d_{H0} - u_H)$, and the Coulomb repulsion $V_C(r_C) =$

dx.doi.org/10.1021/jp407836n | J. Phys. Chem. B 2013, 117, 13639−13645

$V_C(d_{C0} - u_L + u_H) = V_C(d_C - u_C)$. Here, $d_{C0} = d_{L0} + d_{H0}$ is the distance between the adjacent oxygen ions at equilibrium without contribution of Coulomb repulsion. The $d_C = d_L + d_H$ denotes the distance at quasi-equilibrium with contribution of Coulomb repulsion. The displacement of $u_C = u_L + \Delta_L - u_H + \Delta_H$ is the change of distance between the adjacent oxygen ions at quasi-equilibrium. The u_L and u_H take the opposite sign because of the O:H and H−O dislocate in the same direction.[18] A harmonic approximation of the potentials at each quasi-equilibrium site by omitting the higher-order terms in their Taylor's series yields

$$\begin{aligned} V &= V_L(r_L) + V_H(r_H) + V_C(r_C) \\ &= \sum_n \left\{ \frac{d^n V_L}{n! dr_L^n}\bigg|_{d_{L0}} (-u_L)^n + \frac{d^n V_H}{n! dr_H^n}\bigg|_{d_{H0}} (u_H)^n \right. \\ &\quad \left. + \frac{d^n V_C}{n! dr_C^n}\bigg|_{d_C} (-u_C)^n \right\} \\ &\approx [V_L(d_{L0}) + V_H(d_{H0}) + V_C(d_C)] - V'_C u_C \\ &\quad + \frac{1}{2}[k_L u_L^2 + k_H u_H^2 + k_C u_C^2] \end{aligned} \tag{4}$$

where $V_x(d_{x0})$, commonly denoted E_{x0}, is the potential well depths ($n = 0$ terms) of the respective bond. Noting that the Coulomb potential never has equilibrium and that the repulsion force is always greater than zero, one can then expand these potentials at their quasi-equilibrium based on harmonic approximation. As will be shown shorty, this on-site harmonic approximation ensures the sufficient accuracy of the potential paths.

In the Taylor series, the terms of $n = 1$ equal zero for the L and the H segment at equilibrium. At quasi-equilibrium, $V'_X(d_X) + V'_C(d_C) = 0$, or $V''_X \cdot u_X + V''_C \cdot u_C = 0$, must meet. Here V_C' denotes the first-order derivative at the quasi-equilibrium position, i.e., $(dV_C/dr_C)|_{d_C}$. Terms of $n = 2$, or the curvatures of the respective potentials, denote the force constants, i.e., $k_x = V'' = d^2V_x/dr_x^2|_{d_{x0}}$ for harmonic oscillators. Terms of $n \geq 3$ are insignificant and omitted.

Substituting eqs 3 and 4 into eq 2 leads to the coupled Lagrangian equation of the O:H−O

$$\begin{aligned} m_L \frac{d^2u_L}{dt^2} + (k_L + k_C)u_L - k_C u_H + k_C(\Delta_L - \Delta_H) - V'_C \\ - f_p = 0 \\ m_H \frac{d^2u_H}{dt^2} + (k_H + k_C)u_H - k_C u_L - k_C(\Delta_L - \Delta_H) + V'_C \\ + f_p = 0 \end{aligned} \tag{5}$$

2.3. Analytical Solutions. A Laplace transformation turns out the following solutions (details are referred to the Supporting Information)

$$\begin{aligned} u_L &= \frac{A_L}{\gamma_L}\sin \gamma_L t + \frac{B_L}{\gamma_H}\sin \gamma_H t \\ u_H &= \frac{A_H}{\gamma_L}\sin \gamma_L t + \frac{B_H}{\gamma_H}\sin \gamma_H t \end{aligned} \tag{6}$$

The respective coefficient denotes the vibrational amplitude. γ_L and γ_H are the vibration angular frequencies of the respective segment, which depend on the force constants and the reduced masses of the oscillators. This set of general solutions indicates that the O:H and the H−O segments share the same form of eigen values of stretching vibration. The force constants k_x and the frequencies ω_x are correlated as follows

$$\begin{aligned} k_{H,L} = 2\pi^2 m_{H,L} c^2(\omega_L^2 + \omega_H^2) - k_C \\ \pm \sqrt{[2\pi^2 m_{H,L} c^2(\omega_L^2 - \omega_H^2)]^2 - m_{H,L} k_C^2 / m_{L,H}} \end{aligned} \tag{7}$$

where c is the velocity of light traveling in vacuum. Omitting the Coulomb repulsion will degenerate the coupled oscillators into the H_2O:H_2O and the H−O independent oscillators with respective vibration frequencies of $(k_L/m_L)^{1/2}$ and $(k_H/m_H)^{1/2}$.

3. RESULTS AND DISCUSSION

3.1. Correlation between the Force Constant and Vibration Frequency. If the ω_L, the ω_H, and the k_C are given, one can obtain the force constants k_x, the potential well depths E_{x0}, and the binding energy E_x at each quasi-equilibrium state of the two parts of the O:H−O bond. The force constant due to Coulomb repulsion is $k_C = (q_\cdot q_-)/(2\pi\varepsilon_r\varepsilon_0 d_C^3)$ at quasi-equilibrium. The $q_\cdot = 2e$ for the electron lone pair, and $q_- = 0.2$ e, is the effective charge referring to our DFT optimizations (see Supporting Information). In this situation, the k_C equals to 0.17 eV/Å^2 at 0 GPa.

Figure 2 shows the functional dependence of the k_L and the k_H on the ω_L and ω_H. The k_L increases from 1.44 to 5.70 eV/Å^2

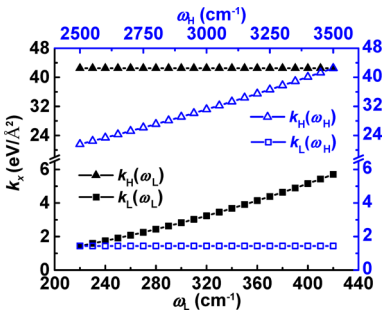

Figure 2. Functional dependence of the force constants k_L and k_H on the vibration frequencies of ω_L and ω_H with $k_C = 0.17$ eV/Å^2. The k_L and the k_H are much more sensitive to their respective frequency increases than the across $k_L(\omega_H)$ and the $k_H(\omega_L)$ that remain almost constant.

while the k_H increases from 21.60 to 42.51 eV/Å^2 with their respective frequency variation. The cross of $k_L(\omega_H)$ and the $k_H(\omega_L)$ remains, however, almost constant. Therefore, eq 7 can be simplified as

$$k_{H,L} = 4\pi^2 c^2 m_{H,L} \omega_{H,L}^2 - k_C$$

or

$$\omega_{H,L} = (2\pi c)^{-1} \sqrt{\frac{k_{H,L} + k_C}{m_{H,L}}} \tag{8}$$

With the measured $\omega_L = 237.42$ cm^{-1} and $\omega_H = 3326.14$ cm^{-1} for the ice-VIII phase under the atmospheric pressure,[3,4,6] eq 7 yields $k_L = 1.70$ eV/Å^2 and $k_H = 38.22$ eV/Å^2. With the known $d_L = 0.1768$ nm and $d_H = 0.0975$ nm under Coulomb

dx.doi.org/10.1021/jp407836n | J. Phys. Chem. B 2013, 117, 13639−13645

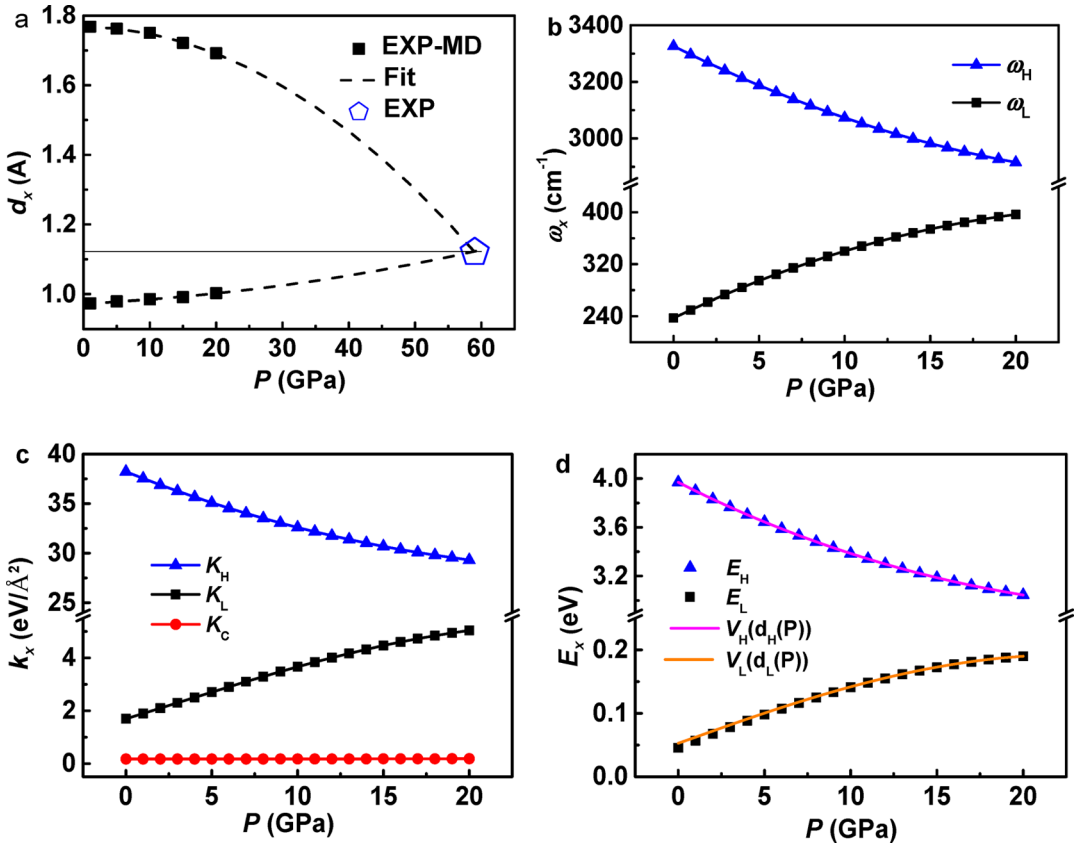

Figure 3. (a) Variation of $d_x(P)$[5,18] (EXP-MD denotes MD derivatives from matching to the measured $V-P$ profile of ice), (b) $\omega_x(P)$,[3−6] (c) force constant $k_x(P)$, and (d) the bond energy $E_x(P)$ of the respective segment of the H-bond of ice under compression. An extrapolation of the $d_x(P)$ to match the measured length symmetry of H-bond at 60 GPa[17] verifies the validity of the $d_x(P)$ profiles. The k_C remains almost constant, making insignificant contribution to the P dependence of k_x. Agreement between the scattered data of harmonic approximation at quasi-equilibrium and the continuum functions $V_x(d_x)$ in (d) verifies the validity of the on-site harmonic approximation. Equations 10 and 11 generalize the pressure dependence of these parameters.

repulsion,[18] one can obtain the free length d_{L0} of 0.1628 nm, and the d_{H0} of 0.0969 nm without involvement of the Coulomb repulsion. Coulomb repulsion lengthens the O---O distance from 0.2597 to 0.2733 nm by 0.0136 nm.

With the derived values of k_L = 1.70 eV/Å^2, k_H = 38.22 eV/Å^2, and E_{H0} = 3.97 eV, we can determine all the parameters in the vdW and the Morse potentials, as well as the force fields of the O:H−O bond at the ambient pressure

$$k_L = 72E_{L0}/{d_{L0}}^2 = 1.70 \text{ eV/Å}^2$$

$$k_H = 2\alpha^2 E_{H0} = 38.22 \text{ eV/Å}^2$$

or

$$E_{L0} = 1.70 \times 1.628^2/72 = 0.062 \text{ eV}$$

$$\alpha = (38.22/3.97/2)^{1/2} = 2.19 \text{ Å}^{-1} \quad (9)$$

3.2. Pressure-Dependent d_x, ω_x, k_x, and E_x. Using MD computation (see Supporting Information), we have decomposed the measured $V(P)$ profile of compressed ice[5] into the $d_H(P)$ and the $d_L(P)$ curves.[18] The $d_x(P)$ curves meet at $d_L = d_H$ = 0.11 nm under 59−60 GPa pressure of ice, which matches exactly the measured proton symmetrization of ice.[17,39] This matching indicates that the MD-derived $d_x(P)$ relation represents the true cooperativity of the d_L and the d_H. Equation 10 and Figure 3a, b show the numerical generalization of the pressure-dependent $d_x(P)$ and the measured phonon relaxation dynamics $\omega_x(P)$.[3−6] Using the measured Raman shifts ω_x and the interionic distances d_x as input, we can readily calculate the evolution of the force constant and bond energy of the respective segment of the O:H−O bond, from one quasi-equilibrium to another, under compression based on eq 6; see Table 1 and Figure 3:

$$\begin{pmatrix} d_H/0.9754 \\ d_L/1.7687 \\ \omega_H/3326.140 \\ \omega_L/237.422 \end{pmatrix} = \begin{pmatrix} 1 & 9.510 \times 10^{-2} & 0.2893 \\ 1 & -3.477 \times 10^{-2} & -1.0280 \\ 1 & -0.905 & 1.438 \\ 1 & 5.288 & -9.672 \end{pmatrix} \begin{pmatrix} P^0 \\ 10^{-2}P^1 \\ 10^{-4}P^2 \end{pmatrix} \quad (10)$$

Contribution of the Coulomb interaction proceeds by offsetting the intrinsic force constant only of the oscillators. The measured d_x and the k_x that is available based on the known m_x, k_C, and the measured ω_x, determine the other parameters involved in the respective potentials; see Supporting Information. The force constants and the bond energies can also be formulated as functional dependent on the pressure:

dx.doi.org/10.1021/jp407836n | J. Phys. Chem. B 2013, 117, 13639−13645

Table 1. Pressure Dependence of the O:H−O Segmental Bond Energy (E_x), Force Constant (k_x), and the Deviated Displacement (Δ_x) from the Equilibrium Position[a]

P (GPa)	$-E_L$ (eV)	$-E_H$ (eV)	k_L (eV/Å^2)	k_H (eV/Å^2)	$-\Delta_L$ (10^{-2} nm)	Δ_H (10^{-4} nm)
0	0.046	3.97	1.70	38.22	1.41	6.25
5	0.098	3.64	2.70	35.09	0.78	6.03
10	0.141	3.39	3.66	32.60	0.51	5.70
15	0.173	3.19	4.47	30.69	0.36	5.26
20	0.190	3.04	5.04	29.32	0.27	4.72
30	0.247	2.63	7.21	25.31	0.14	3.85
40	0.250	2.13	8.61	20.49	0.08	3.16
50	0.216	1.65	9.54	15.85	0.05	2.71
60	0.160	1.16	10.03	11.16	0.04	3.35

[a]Subscript x denotes L and H. The measured $d_x(P)$ and $\omega_x(P)$[3−6,18] are used as input in calculations.

$$\begin{pmatrix} k_H/38.223 \\ k_L/1.697 \\ E_H/3.970 \\ E_L/0.046 \end{pmatrix} = \begin{pmatrix} 1 & -1.784 & 3.113 \\ 1 & 13.045 & -15.258 \\ 1 & -1.784 & 3.124 \\ 1 & 25.789 & -49.206 \end{pmatrix} \begin{pmatrix} P^0 \\ 10^{-2}P^1 \\ 10^{-4}P^2 \end{pmatrix} \quad (11)$$

Results shown in Figure 3c indicate that the k_C (curvature of the Coulomb potential) keeps almost constant under compression. The k_L increases more rapidly than the k_H reduces because of the coupling of the compression, the repulsion, and the potential disparity of the two segments. Figure 3d indicates that increasing the pressure from 0 to 20 GPa stiffens the O:H bond from 0.046 to 0.190 eV while it softens the H−O bond from 3.97 to 3.04 eV, as a result of repulsion. As given in Table 1, when the pressure is increased to 60 GPa, the k_L = 10.03 eV/Å^2 and k_H = 11.16 eV/Å^2, the E_L recovers slightly.

3.3. Potential Paths for H-Bond Length Symmetrization. Table 1 also shows that compression shortens and stiffens the softer O:H bond, which lengthens and softens the H−O bond through the Coulomb repulsion, which results in the contraction of the O−O distance toward O:H and H−O length symmetrization.[3−6,17,18,36] As the d_L is shortened by 4.3% from 0.1768 to 0.1692 nm, the d_H lengthens by 2.8% from 0.0975 to 0.1003 nm when the pressure is increased from 0 to 20 GPa.[18] When the pressure goes up to 60 GPa, the O:H bond almost equals to the elongated H−O bond in length of about 0.11 nm, forming a symmetric O:H−O bond. Results indicate that the nature of the interaction within the segment remains though each of the length and force constant approaches to equality, which means that the sp^3-hybridized oxygen could hardly be dehybridized by compression in the ice X phase.

The local, asymmetric, short-range potentials pertaining to the segmented O:H−O bond have thus been resolved and clarified. Figure 4 shows the $V_x(r)$ paths for the O:H−O bond length symmetrization in compressed ice. Both oxygen ions move first outward from their ideal equilibrium because of Coulomb repulsion. Upon being compressed, both O ions move to the right along the O:H−O with respect to the H coordination origin. The intrinsic equilibrium position of the oxygen in the H−O bond almost superposes on its quasi-equilibrium position, with a displacement of only 6.25 × 10^{-4} nm at first. However, in the O:H, the repulsion-induced displacement of O is 1.41 × 10^{-2} nm, evidencing that the vdW

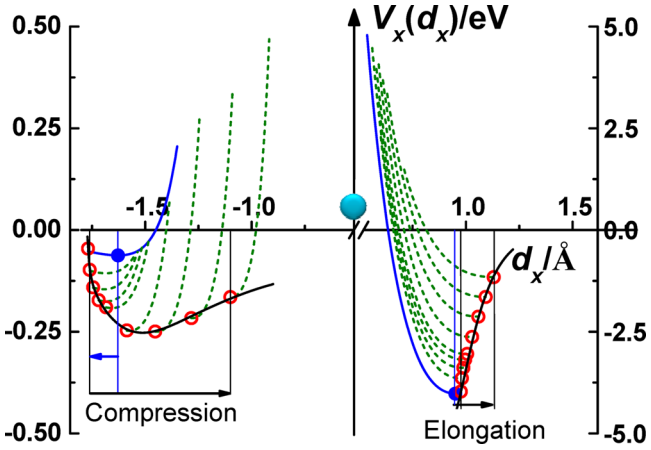

Figure 4. Asymmetric $V_x(r)$ paths for the O:H−O bond length symmetrization of compressed ice (from left to right, P = 0, 5, 10, 15, 20, 30, 40, 50, 60 GPa). The solid blue circles represent the intrinsic equilibrium coordinates (length and energy) of the oxygen ions without the Coulomb repulsion, which satisfy $V'_x(r) = 0$. The open red circles in the leftmost denote the quasi-equilibrium coordinates caused by both the Coulomb repulsion and the pressure, which satisfy $V'_x(r) + V'_c(r) = 0$ and P = 0. The rest of the red circles and the broken curves correspond to $V'_x(r) + V'_c(r) + f_P = 0$, showing the potentials at quasi-equilibrium while the thick solid lines are the contours of the $V_x(r)$ paths. The f_P is the compressing force. Note scale difference between the two segments.

bond is much softer than the H−O bond. The bond energies of both segments relax along the contours as a result of the Coulomb repulsion and external compression. The dislocation steps (10^{-4} nm for H−O and 10^{-2} nm for O:H) of O atoms due to the resultant of compression, repulsion, and deformation resistance are within the limit of fluctuation[53] and they are too small to be detected in reality. However, the sum of these mall steps turned out the final proton symmetrization of ice under compression.

3.4. Significance of the Asymmetric Short-Range Potentials. The $V_x(r)$ paths could be intrinsic, which is less dependent on the applied pressure that serves as a probe only. The current understanding of short-range interactions and intermolecular repulsion could be applicable to the following important findings. First, compression stiffens the softer phonons (110−290 cm^{-1}) and meanwhile softens the stiffer phonons (~3000 cm^{-1}) of organic molecular crystals containing N, H, and O atoms.[54] This asymmetric phonon relaxation dynamics is the same as that of compressed ice.[16] Raman spectral measurements[54] revealed the coupled ω_L stiffening and ω_H softening, of the N−H:O bonds in oxamide under compression. The P-trends of the Raman shifts of melamine−boric acid adduct ($C_3N_6H_6{\cdot}2H_3BO_3$) supermolecules,[55] are the same to that of ice under compression. Compression at pressure greater than 150 GPa also softens the phonons (~4000 cm^{-1}) of hydrogen crystal at various temperatures.[56] These findings may be indicative that the short-range inter- and intramolecular interactions and the interelectron repulsion exist in such crystals. Particularly, nonbonding electron lone pairs are associated not only with oxygen[57] but also with nitrogen and fluorine.[58] Second, the interelectron-pair Coulomb repulsion can be modulated by salting,[10,12,59−62] sugaring,[63,64] heating,[10,65] and electric[66−71] and magnetic[72] fields. According to the present understanding, weakening the repulsion will shorten the H−O bond and

dx.doi.org/10.1021/jp407836n | J. Phys. Chem. B 2013, 117, 13639−13645

deepen its potential to raise the melting point and stiffening the high-frequency phonons.

4. CONCLUSIONS

A combination of the Lagrangian mechanics of oscillator vibration, MD decomposition of volume evolution, and Raman spectroscopy of phonon relaxation has enabled probing of the $V_H(r)$ and the $V_L(r)$ potential paths for H-bond length symmetrization in ice under compression. This analytical solution has enabled us to determine the bond energy, force constant, and potential field of each segment and their pressure dependence based on the measurements. This practice has clarified the presence and significance of the short-range interactions in the flexible, polarizable H-bond, which could be useful to other situations containing bonding and nonbonding interactions. The immediacy of the off and on of the short-range potentials at the boundary is critical and essential while the long-range interactions serve as the background. The findings should be helpful in understanding of water and ice under various conditions.

■ ASSOCIATED CONTENT

Ⓢ Supporting Information

Supporting information describing background information and details of Lagrangian−Laplace solution. This material is available free of charge via the Internet at http://pubs.acs.org.

■ AUTHOR INFORMATION

Corresponding Author

*Tel.: 65 67904517. E-mail: Ecqsun@ntu.edu.sg.

Notes

The authors declare no competing financial interest.

■ ACKNOWLEDGMENTS

Financial support from National Natural Science Foundation (No. 21273191) of China is acknowledged.

■ REFERENCES

(1) Medcraft, C.; McNaughton, D.; Thompson, C. D.; Appadoo, D. R. T.; Bauerecker, S.; Robertson, E. G. Water Ice Nanoparticles: Size and Temperature Effects on the Mid-Infrared Spectrum. *Phys. Chem. Chem. Phys.* **2013**, *15*, 3630−3639.

(2) Petkov, V.; Ren, Y.; Suchomel, M. Molecular Arrangement in Water: Random but Not Quite. *J. Phys: Condens. Matter* **2012**, *24*, 155102.

(3) Pruzan, P.; Chervin, J. C.; Wolanin, E.; Canny, B.; Gauthier, M.; Hanfland, M. Phase Diagram of Ice in the Vii-Viii-X Domain. Vibrational and Structural Data for Strongly Compressed Ice Viii. *J. Raman Spectrosc.* **2003**, *34*, 591−610.

(4) Song, M.; Yamawaki, H.; Fujihisa, H.; Sakashita, M.; Aoki, K. Infrared Absorption Study of Fermi Resonance and Hydrogen-Bond Symmetrization of Ice up to 141 GPa. *Phys. Rev. B* **1999**, *60*, 12644.

(5) Yoshimura, Y.; Stewart, S. T.; Somayazulu, M.; Mao, H.; Hemley, R. J. High-Pressure X-Ray Diffraction and Raman Spectroscopy of Ice Viii. *J. Chem. Phys.* **2006**, *124*, 024502.

(6) Yoshimura, Y.; Stewart, S. T.; Somayazulu, M.; Mao, H. K.; Hemley, R. J. Convergent Raman Features in High Density Amorphous Ice, Ice Vii, and Ice Viii under Pressure. *J. Phys. Chem. B* **2011**, *115*, 3756−3760.

(7) Tsai, M. K.; Kuo, J. L.; Lu, J. M. The Dynamics and Spectroscopic Fingerprint of Hydroxyl Radical Generation through Water Dimer Ionization: Ab Initio Molecular Dynamic Simulation Study. *Phys. Chem. Chem. Phys.* **2012**, *14*, 13402−13408.

(8) Ostmeyer, J.; Chakrapani, S.; Pan, A. C.; Perozo, E.; Roux, B. Recovery from Slow Inactivation in K Channels Is Controlled by Water Molecules. *Nature* **2013**, *501*, 121−124.

(9) Pauling, L. The Structure and Entropy of Ice and of Other Crystals with Some Randomness of Atomic Arrangement. *J. Am. Chem. Soc.* **1935**, *57*, 2680−2684.

(10) Sun, Q. Raman Spectroscopic Study of the Effects of Dissolved Nacl on Water Structure. *Vib. Spectrosc.* **2012**, *62*, 110−114.

(11) Sun, C. Q.; Zhang, X.; Fu, X.; Zheng, W.; Kuo, J.-l.; Zhou, Y.; Shen, Z.; Zhou, J. Density and Phonon-Stiffness Anomalies of Water and Ice in the Full Temperature Range. *J. Phys. Chem. Lett.* **2013**, *4*, 3238−3244.

(12) Park, S.; Fayer, M. D. Hydrogen Bond Dynamics in Aqueous Nabr Solutions. *Proc. Natl. Acad. Sci. U.S.A.* **2007**, *104*, 16731−16738.

(13) Wang, C.; Lu, H.; Wang, Z.; Xiu, P.; Zhou, B.; Zuo, G.; Wan, R.; Hu, J.; Fang, H. Stable Liquid Water Droplet on a Water Monolayer Formed at Room Temperature on Ionic Model Substrates. *Phys. Rev. Lett.* **2009**, *103*, 137801−137804.

(14) Sun, C. Q.; Zhang, X.; Zhou, J.; Huang, Y.; Zhou, Y.; Zheng, W. Density, Elasticity, and Stability Anomalies of Water Molecules with Fewer Than Four Neighbors. *J. Phys. Chem. Lett.* **2013**, *4*, 2565−2570.

(15) Wang, Z.; Wang, F. C.; Zhao, Y. P. Tap Dance of a Water Droplet. *Proc. R. Soc. A: Math., Phys. Eng. Sci.* **2012**, *468*, 2485−2495.

(16) Yoshimura, Y.; Stewart, S. T.; Mao, H. K.; Hemley, R. J. In Situ Raman Spectroscopy of Low-Temperature/High-Pressure Transformations of H_2O. *J. Chem. Phys.* **2007**, *126*, 174505.

(17) Benoit, M.; Marx, D.; Parrinello, M. Tunnelling and Zero-Point Motion in High-Pressure Ice. *Nature* **1998**, *392*, 258−261.

(18) Sun, C. Q.; Zhang, X.; Zheng, W. T. Hidden Force Opposing Ice Compression. *Chem Sci* **2012**, *3*, 1455−1460.

(19) Alejandre, J.; Chapela, G. A.; Saint-Martin, H.; Mendoza, N. A Non-Polarizable Model of Water That Yields the Dielectric Constant and the Density Anomalies of the Liquid: Tip4q. *Phys. Chem. Chem. Phys.* **2011**, *13*, 19728−19740.

(20) Knight, C.; Singer, S. J. Hydrogen Bond Ordering in Ice V and the Transition to Ice Xiii. *J. Chem. Phys.* **2008**, *129*, 164513.

(21) Kumar, R.; Schmidt, J. R.; Skinner, J. L. Hydrogen Bonding Definitions and Dynamics in Liquid Water. *J. Chem. Phys.* **2007**, *126*, 204107.

(22) Vega, C.; Abascal, J. L. F. Simulating Water with Rigid Nonpolarizable Models: A General Perspective. *Phys. Chem. Chem. Phys.* **2011**, *13*, 19663−19688.

(23) Kuball, M.; Hayes, J. M.; Shi, Y.; Edgar, J. H.; Prins, A. D.; van Uden, N. W. A.; Dunstan, D. J. Raman Scattering Studies on Single-Crystalline Bulk Aln: Temperature and Pressure Dependence of the Aln Phonon Modes. *J. Cryst. Growth* **2001**, *231*, 391−396.

(24) Johari, G. P.; Andersson, O. Vibrational and Relaxational Properties of Crystalline and Amorphous Ices. *Thermochim. Acta* **2007**, *461*, 14−43.

(25) Kropman, M. F.; Nienhuys, H. K.; Woutersen, S.; Bakker, H. J. Vibrational Relaxation and Hydrogen-Bond Dynamics of Hdo:H_2o. *J. Phys. Chem. A* **2001**, *105*, 4622−4626.

(26) Yeremenko, S.; Pshenichnikov, M. S.; Wiersma, D. A. Hydrogen-Bond Dynamics in Water Explored by Heterodyne-Detected Photon Echo. *Chem. Phys. Lett.* **2003**, *369*, 107−113.

(27) Hant, W. G.; Zhang, C. T. A Theory of Non-Linear Stretch Vibrations of Hydrogen Bonds. *J. Phys.: Condens. Matter* **1991**, *3*, 27−35.

(28) Urbic, T.; Dill, K. A. A Statistical Mechanical Theory for a Two-Dimensional Model of Water. *J. Chem. Phys.* **2010**, *132*, 224507.

(29) Mahoney, M. W.; Jorgensen, W. L. A Five-Site Model for Liquid Water and the Reproduction of the Density Anomaly by Rigid, Nonpolarizable Potential Functions. *J. Chem. Phys.* **2000**, *112*, 8910−8922.

(30) Mark, P.; Nilsson, L. Structure and Dynamics of the Tip3p, Spc, and Spc/E Water Models at 298 K. *J. Phys. Chem. A* **2001**, *105*, 9954−9960.

(31) Agarwal, M.; Alam, M. P.; Chakravarty, C. Thermodynamic, Diffusional, and Structural Anomalies in Rigid-Body Water Models. *J. Phys. Chem. B* **2011**, *115*, 6935−6945.
(32) Mahoney, M. W.; Jorgensen, W. L. Quantum, Intramolecular Flexibility, and Polarizability Effects on the Reproduction of the Density Anomaly of Liquid Water by Simple Potential Functions. *J. Chem. Phys.* **2001**, *115*, 10758−10768.
(33) Price, D. J.; Brooks, C. L. A Modified Tip3p Water Potential for Simulation with Ewald Summation. *J. Chem. Phys.* **2004**, *121*, 10096−10103.
(34) Ortmann, F.; Bechstedt, F.; Schmidt, W. G. Semiempirical Van Der Waals Correction to the Density Functional Description of Solids and Molecular Structures. *Phys. Rev. B* **2006**, *73*, 205101.
(35) Perdew, J. P.; Wang, Y. Accurate and Simple Analytic Representation of the Electron-Gas Correlation-Energy. *Phys. Rev. B* **1992**, *45*, 13244−13249.
(36) Loubeyre, P.; LeToullec, R.; Wolanin, E.; Hanfland, M.; Husermann, D. Modulated Phases and Proton Centring in Ice Observed by X-Ray Diffraction up to 170 GPa. *Nature* **1999**, *397*, 503−506.
(37) Teixeira, J. High-Pressure Physics - the Double Identity of Ice X. *Nature* **1998**, *392*, 232−233.
(38) Holzapfel, W. On the Symmetry of the Hydrogen Bonds in Ice Vii. *J. Chem. Phys.* **1972**, *56*, 712.
(39) Goncharov, A. F.; Struzhkin, V. V.; Mao, H.-k.; Hemley, R. J. Raman Spectroscopy of Dense H_2O and the Transition to Symmetric Hydrogen Bonds. *Phys. Rev. Lett.* **1999**, *83*, 1998−2001.
(40) Wernet, P.; Nordlund, D.; Bergmann, U.; Cavalleri, M.; Odelius, M.; Ogasawara, H.; Naslund, L. A.; Hirsch, T. K.; Ojamae, L.; Glatzel, P. The Structure of the First Coordination Shell in Liquid Water. *Science* **2004**, *304*, 995−999.
(41) Soper, A. K. An Asymmetric Model for Water Structure. *J. Phys.: Condens. Matter* **2005**, *17*, S3273−S3282.
(42) Wikfeldt, K. T.; Leetmaa, M.; Ljungberg, M. P.; Nilsson, A.; Pettersson, L. G. M. On the Range of Water Structure Models Compatible with X-Ray and Neutron Diffraction Data. *J. Phys. Chem. B* **2009**, *113*, 6246−6255.
(43) Leetmaa, M.; Wikfeldt, K. T.; Ljungberg, M. P.; Odelius, M.; Swenson, J.; Nilsson, A.; Pettersson, L. G. M. Diffraction and Ir/Raman Data Do Not Prove Tetrahedral Water. *J. Chem. Phys.* **2008**, *129*, 084502.
(44) Nilsson, A.; Pettersson, L. G. M. Perspective on the Structure of Liquid Water. *Chem. Phys.* **2011**, *389*, 1−34.
(45) Kuhne, T. D.; Khaliullin, R. Z. Electronic Signature of the Instantaneous Asymmetry in the First Coordination Shell of Liquid Water. *Nat. Commun.* **2013**, *4*, 1450.
(46) Hand, L. N.; Finch, J. D. *Analytical Mechanics*; Cambridge University Press: Cambridge, UK, 2008.
(47) Goldstein, H. *Classical Mechanics*, 3rd ed.; Addison-Wesley: Boston, 2001.
(48) Menzel, D. H. *Fundamental Formulas of Physics*, 2nd ed.; Courier Dover: Mineola, NY, 1960.
(49) Liu, Y.; Wu, J. Communication: Long-Range Angular Correlations in Liquid Water. *J. Chem. Phys.* **2013**, *139*, 041103.
(50) Li, X. Z.; Walker, B.; Michaelides, A. Quantum Nature of the Hydrogen Bond. *Proc. Natl. Acad. Sci. U.S.A.* **2011**, *108*, 6369−6373.
(51) McGuire, R. F.; Momany, F. A.; Scheraga, H. A. Energy Parameters in Polypeptides. V. An Empirical Hydrogen Bond Potential Function Based on Molecular Orbital Calculations. *J. Phys. Chem.* **1972**, *76*, 375−393.
(52) Kumagai, N.; Kawamura, K.; Yokokawa, T. An Interatomic Potential Model for H2o: Applications to Water and Ice Polymorphs. *Mol. Simul.* **1994**, *12*, 177−186.
(53) Skinner, L. B.; Huang, C.; Schlesinger, D.; Pettersson, L. G.; Nilsson, A.; Benmore, C. J. Benchmark Oxygen-Oxygen Pair-Distribution Function of Ambient Water from X-Ray Diffraction Measurements with a Wide Q-Range. *J. Chem. Phys.* **2013**, *138*, 074506.
(54) Yan, T.; Li, S.; Wang, K.; Tan, X.; Jiang, Z.; Yang, K.; Liu, B.; Zou, G.; Zou, B. Pressure-Induced Phase Transition in N-H···O Hydrogen-Bonded Molecular Crystal Oxamide. *J. Phys. Chem. B* **2012**, *116*, 9796−9802.
(55) Wang, K.; Duan, D.; Wang, R.; Lin, A.; Cui, Q.; Liu, B.; Cui, T.; Zou, B.; Zhang, X.; Hu, J. Stability of Hydrogen-Bonded Supramolecular Architecture under High Pressure Conditions: Pressure-Induced Amorphization in Melamine-Boric Acid Adduct. *Langmuir* **2009**, *25*, 4787−4791.
(56) Zha, C.-S.; Liu, Z.; Hemley, R. Synchrotron Infrared Measurements of Dense Hydrogen to 360 gpa. *Phys. Rev. Lett.* **2012**, *108*, 146402.
(57) Sun, C. Q. Oxidation Electronics: Bond-Band-Barrier Correlation and Its Applications. *Prog. Mater Sci.* **2003**, *48*, 521−685.
(58) Sun, C. Q. Dominance of Broken Bonds and Nonbonding Electrons at the Nanoscale. *Nanoscale* **2010**, *2*, 1930−1961.
(59) Aliotta, F.; Pochylski, M.; Ponterio, R.; Saija, F.; Salvato, G.; Vasi, C. Structure of Bulk Water from Raman Measurements of Supercooled Pure Liquid and Licl Solutions. *Phys. Rev. B* **2012**, *86*, 134301.
(60) Park, S.; Ji, M. B.; Gaffney, K. J. Ligand Exchange Dynamics in Aqueous Solution Studied with 2dir Spectroscopy. *J. Phys. Chem. B* **2010**, *114*, 6693−6702.
(61) Gaffney, K. J.; Ji, M.; Odelius, M.; Park, S.; Sun, Z. H-Bond Switching and Ligand Exchange Dynamics in Aqueous Ionic Solution. *Chem. Phys. Lett.* **2011**, *504*, 1−6.
(62) Kim, J. S.; Yethiraj, A. The Effect of Salt on the Melting of Ice: A Molecular Dynamics Simulation Study. *J. Chem. Phys.* **2008**, *129*, 124504.
(63) Saldaña, M. D. A.; Alvarez, V. H.; Haldar, A. Solubility and Physical Properties of Sugars in Pressurized Water. *J. Chem. Thermodyn.* **2012**, *55*, 115−123.
(64) Imperato, G.; Eibler, E.; Niedermaier, J.; Konig, B. Low-Melting Sugar-Urea-Salt Mixtures as Solvents for Diels-Alder Reactions. *Chem. Commun.* **2005**, 1170−1172.
(65) Cross, P. C.; Burnham, J.; Leighton, P. A. The Raman Spectrum and the Structure of Water. *J. Am. Chem. Soc.* **1937**, *59*, 1134−1147.
(66) Qiu, H.; Guo, W. Electromelting of Confined Monolayer Ice. *Phys. Rev. Lett.* **2013**, *110*, 195701.
(67) Ehre, D.; Lavert, E.; Lahav, M.; Lubomirsky, I. Water Freezes Differently on Positively and Negatively Charged Surfaces of Pyroelectric Materials. *Science* **2010**, *327*, 672−675.
(68) Svishchev, I. M.; Kusalik, P. G. Electrofreezing of Liquid Water: A Microscopic Perspective. *J. Am. Chem. Soc.* **1996**, *118*, 649−654.
(69) Zangi, R.; Mark, A. E. Electrofreezing of Confined Water. *J. Chem. Phys.* **2004**, *120*, 7123−7130.
(70) Choi, E.-M.; Yoon, Y.-H.; Lee, S.; Kang, H. Freezing Transition of Interfacial Water at Room Temperature under Electric Fields. *Phys. Rev. Lett.* **2005**, *95*, 085701.
(71) Rzesanke, D.; Nadolny, J.; Duft, D.; Muller, R.; Kiselev, A.; Leisner, T. On the Role of Surface Charges for Homogeneous Freezing of Supercooled Water Microdroplets. *Phys. Chem. Chem. Phys.: PCCP* **2012**, *14*, 9359−9363.
(72) Zhang, G.; Zhang, W.; Dong, H. Magnetic Freezing of Confined Water. *J. Chem. Phys.* **2010**, *133*, 134703.